CHAPTER 3
THEORY OF EXPERIMENTAL AND ANALYTICAL TECHNIQUES

3.1 Introduction

In this chapter, several theories of experimental study and analytical techniques used to characterize the samples are detailed out. To begin with, the design of experiment that is used to optimize the conditions of synthesized catalyst, carbon nanotubes and graphitic nanofibers are elaborated. This is followed by the theory used in the analyses which are signal-to-noise ratio and analysis of variance. For isotherm modelling purpose, the Neuro-fuzzy model is introduced. Next, theory of adsorption, types of adsorption isotherm and the principle of magnetic suspension balance as the gravimetric measurement instrument of adsorption are explained. At the end, the theory and principles of several instruments used to characterize the developed samples such as transmission electron microscope, scanning electron microscope, Raman spectroscopy and x-ray diffractometer are included in this chapter.

3.2 Design of experiment: Taguchi Method

Design of experiment (DOE) was first introduced by Sir Ronald A. Fisher in 1920s in England for agricultural experiment. It was developed to determine the relationship between the different factors affecting a process and the output of that process. DOE theory starts with the assumption that all inputs might be interacting with all other inputs at the same time. The investigation of looking at all possible interactions is called full factorial DOEs (Cesarone, 2001).

Later in 1940s Dr Genechi Taguchi proved that DOE could be used not just to improve quality (consistency of performance) but also quantify the improvements. This is happened when he introduced Taguchi method as he was trying to improve the quality of manufactured products after World War II (Roy, 2001). Taguchi method is an experiment design technique or Robust Design which is designed to achieve reduced variation. This is done by moving the mean performance to the target a well as by reducing variations around the target. Today, this technique as been applied to improve the quality of manufactured goods, biotechnology, marketing and advertising. It reduces scrap work, rework costs and manufacturing costs due to excess variability in processes (Antony et al., 2001).

Basically, Taguchi method is a combination of mathematical and statistical techniques used in an empirical study (Hung et al., 2001). Compare with conservative factorial design, fewer experiments are required in order to study all levels of input parameters. This is done by filtering out some effects due to statistical variation.

There are five major phases in DOE of Taguchi as described by (Roy, 2001). These include planning, designing and conducting the experiments as well as analyzing and confirming the results. Planning the experiments is done to agree on objectives and identify factors and levels while designing the experiments is needed to determine the number of experiments to run. Conducting the experiments is achieved by following the sequence of running the experiments. In order to determine the optimum design condition and influence of factors, analysis of the results is done. This is followed by verifying the results predicted as to confirm the results.

In order to make the DOE technique more applicable that is to reduce the size of experiments, fractional factorial experiments and orthogonal arrays were developed. An orthogonal array (OA) means that factors can be evaluated independently of one another. i.e. the effect of one factor does not bother the estimation of the effect of another factor (Ross, 1996). OA allows one to compute the main and interaction effects via a minimum number of experiment trials.

Factor is any input side of a system that has an influence on the performance of the product or process. It is also known as input, variable, parameter, ingredient, cause or constituent. Factors can be classified into two types (Roy, 2001):

a) A continuous factor – Possibility to adjust the values in a continuous manner to carry out experiment. For example, temperature, reaction time, gas flowrate, etc.

b) A discrete factor – Also known as fixed actor, it is applied when it is not quantifiable and can only jump from one state to another. For example, type of catalyst, type of reactor, type of gas, etc.

Selection of OA depends on number of factors and interaction of interest, number of levels for the factors of interest and the desired of experimental resolution or cost limitation. OA is designated by the notation *L* (*L* for Latin squares) with a subscript or dash (L_4 or *L*-4) (Roy, 2001). The subscript refers to number of rows in the table, which indicates the number of combinations the design will prescribe. OA can be designed in two-level factors such as L_4, L_8, L_{12}, L_{16}, L_{32} and three-level factors such as L_9, L_{18}, L_{27}.

OA is preferred for experimental designs because they are more likely to produce reproducible results. Result which is also known as output or responses are a measure of performance. It can be expressed as numerical data or attribute data. Numerical data can be classified as objective and subjective (Roy, 2001). The former is where the performance is measurable in terms of number. For example weight, thickness, strength, etc. The latter performance is evaluated in a scale of 0 to 10. Attribute data is where performance is evaluated as *good*, *average*, *poor*, etc.

Quality characteristic (QC) refers to the measured results of the experiment. It can also refer to their nature of the performance objectives such as bigger is better, smaller is better, and normal is the best. In order to measure the performance of a population′s test samples in terms of its consistency, a quantity called *mean-squared deviation* (MSD) as been defined as below (Roy, 2001):

Target: $\text{MSD} = \sigma^2 + \left(Y_{avg} - Y_0\right)$ (3.1)

where σ is the standard deviation, Y_{avg} is the average value and Y_0 is the target value. For smaller or bigger QC, MSD is written as below (Roy, 2001):

$$\text{Smaller: MSD} = \frac{Y_1^2 + Y_2^2 + Y_3^2 + ...Y_n^2}{n} \tag{3.2}$$

$$\text{Bigger: MSD} = \frac{1/Y_1^2 + 1/Y_2^2 + 1/Y_3^2 + ...1/Y_n^2}{n} \tag{3.3}$$

Taguchi recommends the use of signal-to-noise ratio (*SNR*). This is done to maximize the performance of a system or product by minimizing the effect of noise while maximizing the mean performance. *SNR* is treated as a response or output of the experiment which is a measure of variation when uncontrolled noise factors are present in the system (Antony et al., 2001). The ratio is expressed as a log transformation of the MSD. It should be performed when more than one sample is tested in each trial condition. *SNR* can be expressed as $-\log_{10}$MSD. The negative sign is applied purposefully that is to ensure that *SNR* increases for decreasing MSD. Thus, for all QCs of the original results, lower MSD and higher *SNR* values will be desirable.

Several works have been done by implementing Taguchi approach for their CVD experimental method. For example, Taguchi method with L_{18} OA was used to investigate the effect of various factors and performance of microwave plasma enhanced CVD diamond films. They used 8 two-level factors, and they analyze the bigger-the-better response of Raman peaks FWHM that represents crystallinity of diamond films (Hung et al., 2001). Another study has used L_{16} OA which is 5 four-level factors to produce nanocrystalline diamond (NCD) using time-modulated CVD process (Ahmed et al., 2006; Ali et al., 2004).

Some researchers preferred to have less parameters in their experiments. For example Taguchi design with L_9 OA (3 three-level factors) was implemented to prepare nanosized silver particle using chemical reduction method (Kim et al., 2004). Synthesis of CNT was done using thermal CVD by using Taguchi approach of L_9 OA which is 4 three-level factors. *SNR* was done where the smaller-is-better

analysis of CNT diameter and the larger-is-better analysis of the CNT evaluations using SEM (Porro et al., 2006). CNT prepared by microwave plasma-enhanced chemical vapour deposition (MPCVD) was done using Taguchi method with L_9 OA which is 5 three-level factors. Threshold voltage was selected as the smaller-the-better response and emission current density was selected as the bigger-the-better response (Ting et al., 2006).

3.3 Analysis of variance

Apart from *SNR*, the main effects of the process parameters are analyzed using Taguchi DOE software that is Qualitek-4 (QT4) version 14.7.0. The Qualitek-4 calculates the performance based from analysis of variance (ANOVA). ANOVA was first introduced by Sir Ronald Fisher in the 1930s as a statistical method that is used to interpret experimental data (Ross, 1996; Roy, 2001). The results are in the form of statistical table which displays relative influence of factor that assigned to the column of the OA. Apart from ANOVA, Qualitek-4 also determines the optimum conditions of the experimental study based from the ANOVA results.

In ANOVA output table (as in Appendix A), the first column or section prints degrees of freedom, *df* is equal to the number of independent pieces of information concerning the variance. If N is the total number of data points (or pieces of information) and M is the number of factor levels, thus, *df* (factor) that correspond between factor variance is M-1 while *df* (error) that corresponds to residual is N-M. Total degrees of freedom is

$$df = df(\text{factor}) + df(\text{error}) = M - 1 + N - M = N - 1 \tag{3.4}$$

The second column of the ANOVA table prints the total amount of variability or sum of squares (S). For certain source of sum of squares, S_A is calculated as:

$$S_A = \sum_{i=1}^{n} \left(x_i - \bar{x} \right)^2 \tag{3.5}$$

where x_i is i-th response or data and $\bar{x}$ is the mean or average of the data.

The next column prints a mean square or variance (V) where the sum of squares divided by its associated degrees of freedom (Ross, 1996). For certain source of variance, V_A, it can be estimated as:

$$V_A = \frac{\sum_{i=1}^{N}\left(x_i - \bar{x}\right)^2}{N-1} \tag{3.6}$$

The F-ratio or F-value is the test statistic used to decide whether the sample means are within sampling variability of each other (Dallal, 2009). As described by (Stephenson, 2003) values of F close to one indicate that the differences among group means can be attributed to natural or random error variability while values of F much larger than one indicate that some of the groups differ significantly in terms of their mean or average values. The formula is:

$$F = \frac{V_A}{V_e} \tag{3.7}$$

where V_e is the error in variance.

$F_{\alpha;v1;v2}$ is an F value given in Appendix A which is the format in determining an explicit F value where α is the risk where confidence is equal to (1-α), v_1 is degree of freedom associated with the numerator and v_2 is the degrees of freedom associated with denominator (Ross, 1996). If F values exceed some criterion (F values from the table), the factors are believed to influence the average value for the population. On the other hand, if F values less than the criterion, the factors are believed have no effect on the average. The last column represents the percent of contribution, P that is (Ross, 1996):

$$P = \frac{SS_A^{'}}{SS_T} \times 100\% \tag{3.8}$$

where S_T is the total of the sum of squares and S_A' is pure sum of squares can be obtained from

$$SS_A^{'} = SS_A - (df)(V_e) \tag{3.9}$$

P reflects the relative power of a factor and/or interaction to reduce variation (Ross, 1996). The amount of *P* value indicates how much total variation could be reduced. For a high value of *P*, a small variation will have a great influence on the performance. *P* due to error provides the adequacy of the experiment. If the value is small (e.g. less than 15%) then it is assumed that no important factors were omitted and further improvement is not required. However, if the *P* due to error value is high (e.g. more than 50%) then there could be several factors were omitted or the conditions chosen are not precisely controlled. Thus, further improvement or more experimentation is necessary.

3.4 Neuro-fuzzy system

Neuro-fuzzy system is a combination of specific knowledge of fuzzy logic with the learning power of neural network. Neural network is proficient at recognizing patterns but poor at explaining how they reach their decisions (Fuller, 1999). On the other hand, fuzzy logic systems are capable at explaining their decisions, but the rules that are used to make the decisions they are not acquired automatically. Therefore, when these two combine, neural network can learn from data sets while fuzzy logic solutions are easy to verify and optimize.

The neuro-fuzzy modelling describes systems by means of fuzzy *if-then* rules represented in a network structure. In this structure, learning algorithms known from the area of artificial neural network can be applied. The tools for building neuro-fuzzy models are based on combinations of algorithms from the fields of neural networks, pattern recognition and regression analysis. This powerful modelling can facilitate the effective development of models by combining information from different sources, such as empirical models, heuristics and data (Babuska et al., 2003). Neuro-fuzzy is regarded as an assumption-free model because the model does not require any restrictive assumptions of the statistical models (Malhotra et al., 2002).

Neuro-fuzzy model can be regarded as a grey-box technique on the boundary between neural network and qualitative fuzzy model. Fuzzy model can be classified into two categories that are a linguistic model and Sugeno's model. The linguistic model is based on the collection of *if-then* rules with vague predicates and use of a fuzzy reasoning such as Mamdani's model (Arafeh, 1996). In this model, sets of rule operating with liguistic values of input/output variables, appears as an analogy to the system of equations used for presentation of linear and non-linear systems. The meaning of linguistic terms (for example, *Low, Medium, High*) is defined by membership function, which can be defined by the model developer based on prior knowledge or by using data. When input-output data of the system under study are available, the membership function can be constructed or adjusted automatically. For a Two-Input-Single-Output (TISO) system, the model has the form: If x is A and y is B Then z is C. Where A, B, and C are fuzzy sets of the universes of discourse of X, Y and Z, respectively. Sugeno's model has characterized with functional type consequents (Arafeh, 1996). The form of Sugeno's model for a TISO system is: If x is A and y is B Then $z = f(x,y)$. A and B are fuzzy sets of the universes of discourse x and y, respectively, x and y are values of the input variables.

3.5 Adsorption Studies

The term *adsorption* was first used by Kayser in 1881 when he described the increase in concentration of gas molecules in neighbouring solid surfaces (Roque-Malherbe, 2007). Later in 1909, McBain proposed the term 'sorption' to describe mass transport of gases onto a surface solid as well as penetration and condensation of gases within pores (Fletcher, 2008). The following section explains the principles of adsorption including important terminologies in an adsorption process.

3.5.1 Principles of adsorption

Adsorption occurs when a gas molecule comes in contact with a solid surface at suitable conditions of temperature and pressure, the concentration of the gas is greater near the surface than in the bulk of the gas phase (Yates, 1992). The capacity of adsorption depends on several factors such as effectively accessible surface area, the pore size, surface topology, chemical composition of the surface, and the applied pressure and temperature (Yürüm et al., 2009). From Figure 3.1, adsorptives are the gas or liquid molecules that are interacting with the surface atoms of a solid while adsorbates refer to the molecules which are adsorbed on the solid to form a separate phase.

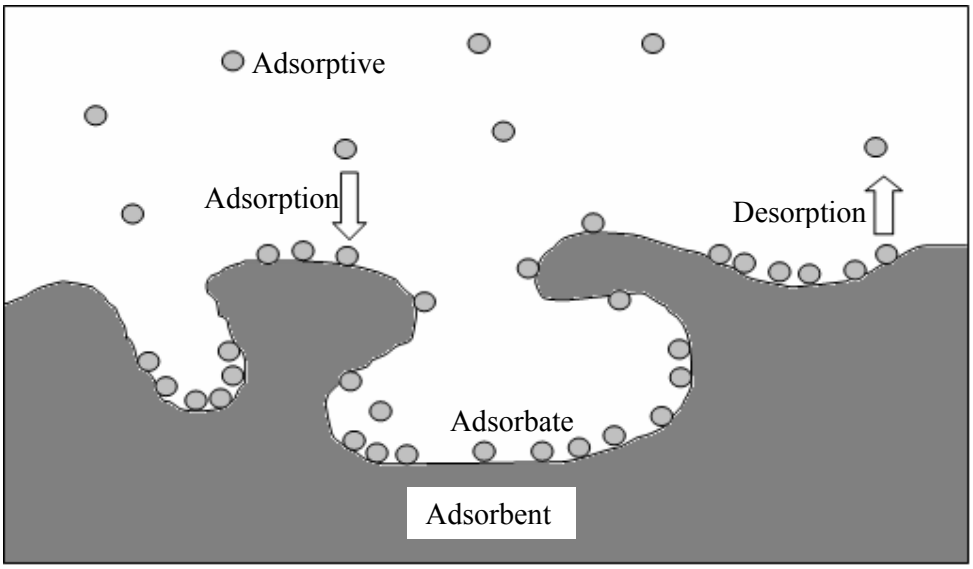

Figure 3.1 Molecular situation of an adsorption system (Keller et al., 2005).

The solid phase with external and internal surfaces exposed to the molecules is known as adsorbent. For physical adsorption, when the condition temperature is increased or the condition pressure is decreased, desorption occurs where the adsorbent return back to the gaseous phase (Keller et al., 2005). An adsorption process can be categorized into physical adsorption (physisorption) and chemical adsorption (chemisorption). Physisorption or van der Waals adsorption is the process when the adsorbed phase in thermodynamic equilibrium with the gas phase due to an attraction between the adsorbate and adsorbent. The attraction is due to the

formation of intermolecular electrostatic like London dispersion forces, van der Waals forces from induced dipole-dipole interactions or physical configuration of the adsorbent porosity (Fletcher, 2008; Roque-Malherbe, 2007). Since no chemical bonds are formed during physisorption, the adsorbate molecules could be reversibly desorbed from the adsorbent.

Chemisorption is a chemical reaction process when the adsorbate molecules are strongly bound to the surface atoms or molecules of the adsorbent due to the transfer of electrons between the adsorbate and the adsorbent. This process is less common as compared with physisorption and the regeneration of adsorbed molecules is difficult or impossible (Fletcher, 2008; Roque-Malherbe, 2007). Comparison between physisorption and chemisorption can be seen in Table 3.1.

Table 3.1 Basic properties of physisorption and chemisorption (Fletcher, 2008; Roque-Malherbe, 2007)

Property	Physisorption	Chemisorption
Heat of adsorption (kJ/mol)	20-40	>80
Adsorption capacity (as T increases)	Decreases	Increases
Desorption	Easy	Difficult or impossible
Bond or attraction	Weak	Strong
Kinetic	Rapid	Slow
Specificity	Non-specific	Very specific
Structure of sorbate	Monolayer, multilayer	Monolayer only
Adsorbent surface	Not altered	Altered

3.5.2 Porosity

Porosity is defined as the ratio of the volume of pores and voids to the volume occupied by the solid. However, it is sometimes difficult to distinguish between

roughness and porosity or between pores and voids. Thus, in principle, the solid is porous when the surface irregularities are deeper than they are wide (Rouquerol et al., 1999). Figure 3.2 clarifies several terms to describe accessibility of porosity such as blind, open, trough, interconnected and closed pores. Apart from that, pores also come in different shapes as indicated in Figure 3.3. These pore shapes can be predicted based on the hysteresis loop that obtained from the adsorption-desorption curves (Lowell et al., 1991).

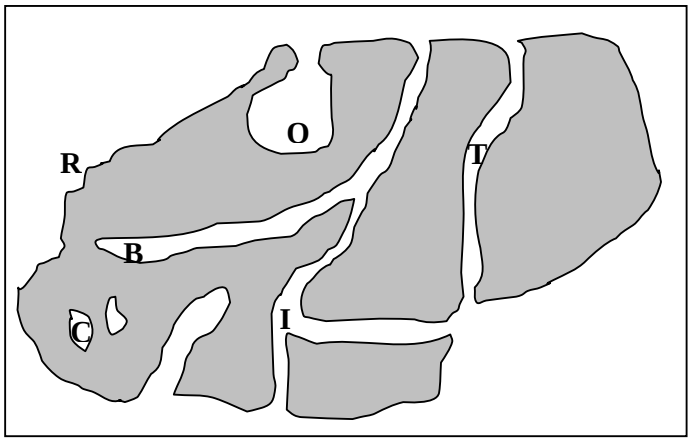

Figure 3.2 Various types of pores: blind (B), open (O), interconnected (I), through (T), closed (C), and also roughness (R) in a cross-section of an example of solid adsorbent (Rouquerol et al., 1999).

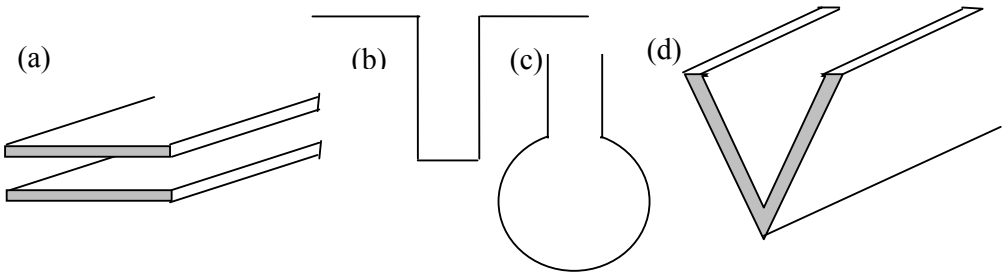

Figure 3.3 Various shapes of pores like (a)slit, (b)cylindrical, (c)ink bottle, and (d)wedges

According to International Union Pure and Applied Chemistry (IUPAC) pores can be classified based on their width as stated in Figure 3.4. A pore diameter smaller

than 2 nm is classified as micropores, mesopores between 2-50 nm and macropores are larger than 50-100 nm. (Willems et al., 2005).

Macropores are formed due to major lattice structure defects like racks, fissures and etching channels while mesopores are the result of solid structure defect which then provides as passages for a transport system for molecules going to the micropores. The micropores are caused by an imperfect stacking of constituent molecules and packing arrangements of the bulk material (Fletcher, 2008) it can be divided into supermicropores and ultramicropores (Inagaki, 2000).

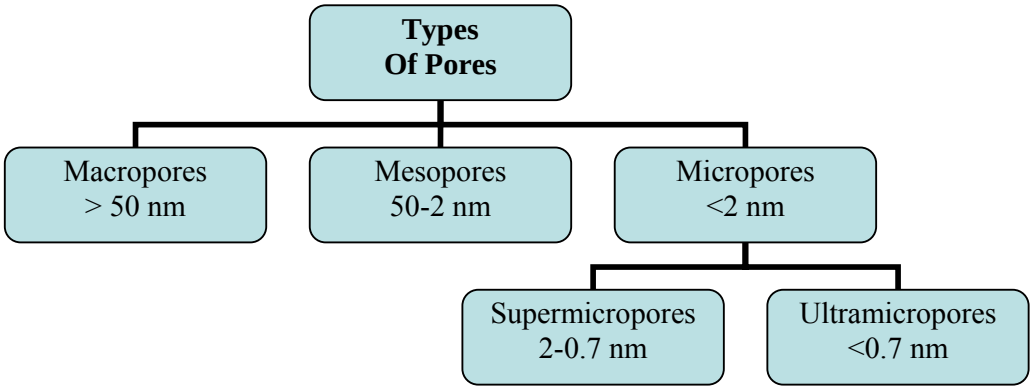

Figure 3.4 Classification of pores (Fletcher, 2008; Inagaki, 2000; Willems et al., 2005)

3.5.3 Types of adsorption isotherms

Adsorption can be described through isotherm that is the quantity of mass adsorbed as a function of its pressure (for gas) or concentration (for liquid) under equilibrium condition at constant temperature (Everett, 2001). The quantity of mass adsorbed is usually normalized by the mass of adsorbent for the ease of comparison among different materials. The term 'adsorption isotherm' was first introduced by Ostwald in 1885 (Kiefer et al., 2008). There are several types of adsorption isotherms which have been recognized earlier by Brunauer, Deming, and Teller as given in Figure 3.5. Type I isotherm is concave to relative pressure axis where it rises sharply at low relative pressure and reaches a plateau, that is the asymptotic value that the

mass adsorbed approaches and maintains at high pressure (Keller et al., 2005). Furthermore, known as Langmuir isotherm, this curve is for typical adsorbents like charcoal, molecular sieve and alumina with a predominantly microporous structure since the majority of micropore filling will occur at low relative pressures (Fletcher, 2008; Nackos, 2006). It is assumed only monolayer adsorption occurs and the surface of adsorbent is homogeneous, i.e. all adsorption sites are energetically identical.

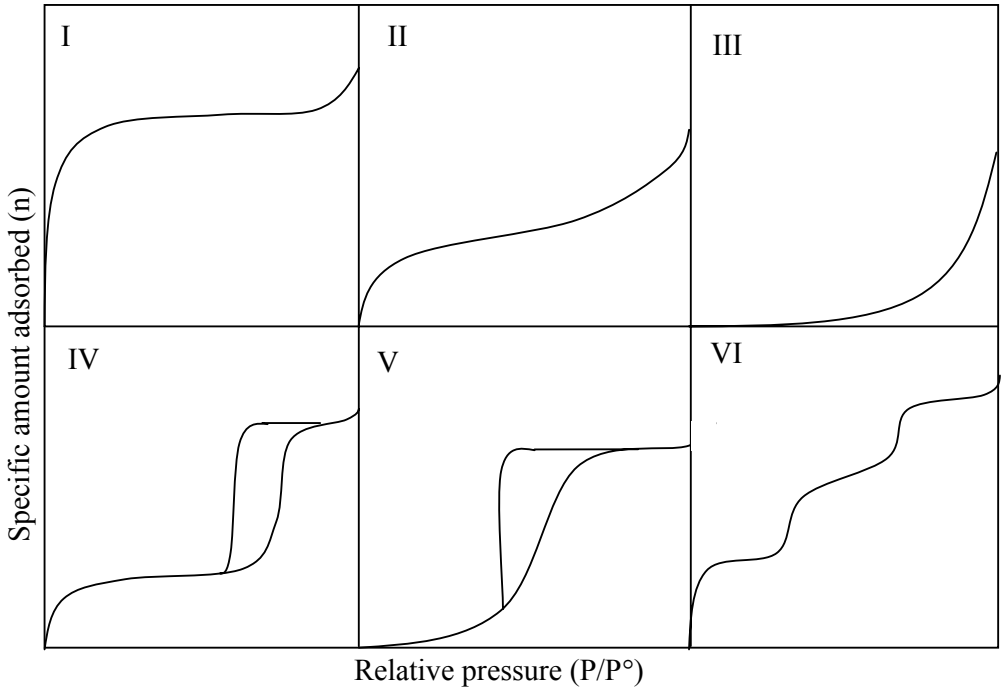

Figure 3.5 Types of adsorption isotherm (Fletcher, 2008; Nackos, 2006)

Type II isotherm describes adsorption in mesoporous materials, where monolayer adsorption occurs at low pressure. It is followed by saturation multilayer of adsorption at higher pressure and pore condensation at the end (Keller et al., 2005). Majority of non-porous material will exhibit Type II with sharp and well-defined knee (Nackos, 2006). This behaviour can be found in carbon material, which has a mixture of micro- and meso- porosity (Fletcher, 2008).

Unlike Type I and Type II, Type III isotherm is convex to the relative pressure axis. It shows a characteristic of adsorbate-sorbent (*a*-*s*) interaction is weaker than adsorbate-adsorbate (*a*-*a*) interaction (Keller et al., 2005). This type of isotherm can

be found in non-porous and microporous adsorbent. Initially the weak *a-s* interaction results in low uptake but as soon as a molecule adsorbed onto an adsorption site, the strong *a-a* interaction provides a driving force for adsorption process i.e. the more molecules adsorb, the easier for further molecules adsorb (Fletcher, 2008; Nackos, 2006). Thus, an accelerated uptake is found at higher pressure. This is an example of non-wetting system such as adsorption of water on a hydrophobic substance like pure charcoal, zeolites, activated carbon (Keller et al., 2005; Yates, 1992).

Type IV isotherm has an initial region similar with Type II but at higher pressure, it tends to level off and later exhibits a hysteresis loop (Rouquerol et al., 1999). The hysteresis loop is due to the act of filling and emptying the mesopores by capillary condensation, a phenomenon where the actual vapor pressure exceeds the equilibrium vapor pressure with porous solids (Bányai et al., 2007). The lower branch represents adsorption while the upper branch represents desorption. Some typical examples for this isotherm type are observed in water vapor from humid air on special activated carbon and hydrophilic zeolites (Keller et al., 2005).

Type V is the most uncommon isotherm. At an initial region, it resembles Type III, which is convex to the relative pressure axis. However, unlike Type III, this isotherm is found in porous solid and exhibit hysteresis loop at higher pressure. Hence, this isotherm type is similar like Type IV which has the characteristic of multilayer adsorption on highly porous adsorbents. The filling of capillaries starts to occur at near saturation vapor pressure, which results in flattening of isotherm (Yates, 1992). Such isotherm trend is found in water adsorption onto special activated carbon and carbon molecular sieves (Keller et al., 2005).

Type IV isotherm is also known as a stepped isotherm. It is associated with layer-by-layer adsorption on a highly uniform surface like planar graphite and alumina silicates (Keller et al., 2005; Rouquerol et al., 1999). The shape is due to the complete formation of monomolecular layers follow by a next progression of a subsequent layer. The isotherms arise from adsorption on extremely homogeneous,

non-porous surfaces where the monolayer capacity corresponds to the step height (Fletcher, 2008) .

3.6 Intelligent gravimetric analyzer

Gravimetric adsorption measurement is a new method which can characterize porous media like specific BET surface area and pore size distribution, measure gas adsorption equilibria and investigate adsorption kinetics. One of the techniques is Intelligent gravimetric analyzer (IGA). IGA is a gravimetric gas sorption analyzer with ultra-sensitive microbalance. It is designed to study single component gas-solid and gas-liquid interaction. The system operates at temperatures from -196 to 1000 °C and at pressures ranging from ultra-high vacuum (UHV) to 20 bar.

The IGA-001 is based on the conventional gravimetric measuring method where to weigh the sample, the measuring cell is in direct contact with the weighing instruments. This instrument has been used in a diverse range of applications areas, including gas sorption on carbons and zeolites, gas interaction with ionic liquids and for the characterisation of hydrogen storage materials (Hiden Isochema, 2009). The amount of gas adsorbed in the IGA experiment is given as (Ansón et al., 2004):

$$w = \Delta w + \Delta V \rho_g \tag{3.10}$$

where w is the total adsorption, Δw is the weight difference measured directly by gravimetry, ΔV is the displaced volume of the sample and ρ_g is the gas phase density (Ansón et al., 2004)

3.7 Magnetic Suspension Balance

The main difficulty when using conventional gravimetric instruments is the direct contact between the measuring cell i.e. sample atmosphere and the weighing instrument. The balance can be damaged or disturbed by the measuring atmosphere since the measuring atmosphere can be adversely affected by flushing gasses and

pollution. These limitations considerably reduce the field of application of conventional measurement devices. To overcome such problems, a reliable suspension balance is introduced so that the sample is weighed contactlessly under nearly all environments. This instrument is known as magnetic suspension balance (MSB) supplied by Rubotherm GmbH from Germany.

In MSB, instead of hanging directly at the balance the sample is linked to a suspension magnet which consists of a permanent magnet, a sensor core and a device for decoupling the measuring load i.e. sample. In addition, an electromagnet, which is attached to the under-floor weighing hook of a balance, maintains a freely suspended state of the suspension magnet via an electronic control unit. By using this magnetic suspension coupling the measurement force is transmitted contactlessly from the measuring chamber to the microbalance, which is located outside the chamber under ambient atmospheric condition. Consequently, this arrangement eliminates almost all restrictions which are inherent to conventional gravimetric measuring instruments. The following section uncovers the experimental setup and the theory behind MSB.

3.7.1 Experimental set up

Magnetic suspension balance (MSB) system consists of a magnetic field that is acting on a permanent magnet as shown in Figure 3.6. This magnet is decoupled by a suspension rod to the sorbent load in order to keep it in balance against gravity so that it floats freely in the sorptive atmosphere. The sorbent is placed in a stainless steel wire cloth basket and attached to a permanent magnet. They are coupled to an electromagnet via an external magnetic field penetrating the adsorption vessel's walls. The electric current in the electromagnets will always keep the permanent magnet, basket and sorbent sample (suspension) floats freely inside the adsorption vessel. Since the stable flotation of the suspension can be measured, the weight of the sample and the mass of sorptive gas adsorbed can be determined. This can be done after appropriate calibration and vacuum measurements are achieved (Keller et al., 2005).

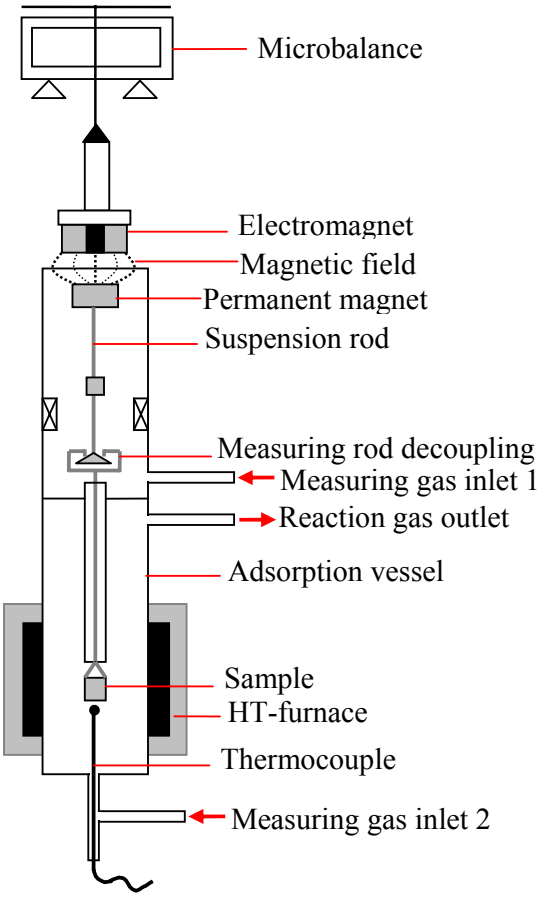

Figure 3.6 Magnetic suspension balance (Keller et al., 2005)

3.7.2 Theory and procedure of MSB

A gravimetric measurement using the MSB can be done by following four principles steps as follow (Rubotherm GmbH, 2005):

3.3.2.1 Blank measurement

Blank measurement is carried out in order to determine the volume of the sample container. Thus, the measurement is done using an empty container by flowing inert gas such as nitrogen. During the measurement, the balance reading (m_{BAL}),

temperature (T) and pressure (P) of the inert gas are recorded. Based on the given T and P, the density of the gas at a specific condition (ρ) can be determined. Later, a graph of m_{BAL} versus ρ is plotted, which gives a linear line with negative slopes as shown in Figure 3.7. This indicates the decrease in mass balance as the density of the gas increases due to buoyancy acting on the sample container. A buoyancy effect (B) which is proportional to the density can be described as below:

$$B = \rho \cdot V \tag{3.11}$$

V is the volume of the body which has been exerted by the buoyancy effect.

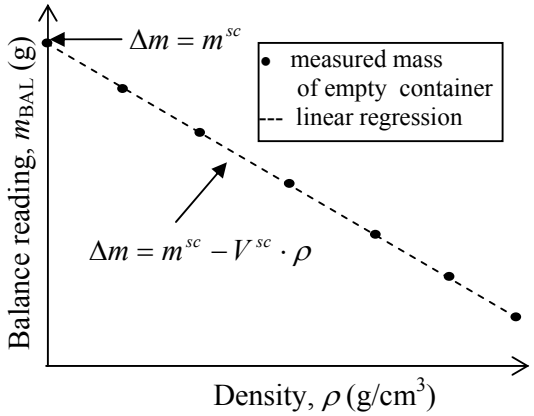

Figure 3.7 Result example of a blank measurement (Rubotherm GmbH, 2005)

The linear regression as been exhibited in Figure 3.8 is known as (Rubotherm GmbH, 2005):

$$\Delta m = m^{sc} - V^{sc} \cdot \rho \tag{3.12}$$

From the equation it can be seen that the slope or gradient of the graph is the volume of the sample container (V^{sc}) while the mass of the container (m^{sc}) is the intersection of the graph at y-axis that is the value of m_{BAL} when ρ is zero.

3.3.2.2 Loading and reactivation of sample

In Rubotherm MSB, the measuring cell is exposed by opening six bolts and nuts before a sample is loaded into the sample container. Then reactivation is done by

applying heat to the sample. The sample is evacuated at the same time. The reactivation is considered to be completed when there is no change in sample mass, m^s measured by the MSB.

3.3.2.3 Buoyancy measurement

It is essential to perform buoyancy measurement in order to determine the mass and the volume of the sample. This is because the mass measured by the MSB during the adsorption measurement needs to be corrected due to the buoyancy effect acting on the sample in the gas phase. The measurement is performed as like measuring adsorption isotherm where a stepwise increase of pressure at constant temperature is performed. The gas used in the measurement is Helium (He) since this gas is unlikely to adsorb onto the sample, and therefore, it does not change the mass sample. A plot of m_{BAL} versus ρ will again give a straight line with negative slope (see Figure 3.8) and the equation of the line is given as:

$$\Delta m = m^{sc} + m^{s} - \left(V^{sc} + V^{s}\right) \cdot \rho \tag{3.13}$$

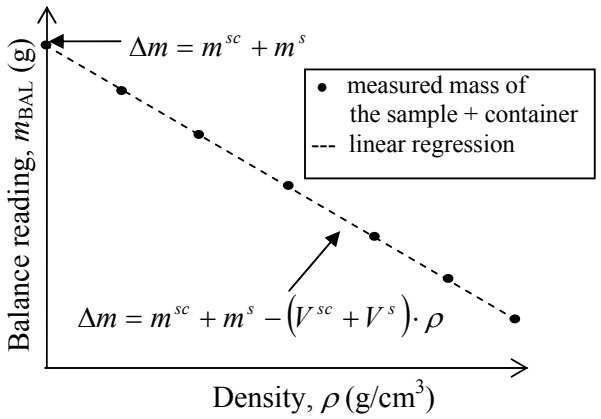

Figure 3.8 Result example of a buoyancy measurement (Rubotherm GmbH, 2005)

The decrease of the measured m_{BAL} (masses of container and the loaded sample) with increasing pressure (density) of the gas phase is due to the buoyancy acting on the sample and the container. From the graph the value of sample volume (V^s) can be calculated from the gradient of the slope (V^{sc}+V^s) and the mass sample (m^s) can

be determined from the intersection at the *y*-axis (m^{sc}+m^{s}). In addition, sample density, ρ^{s} can be estimated once the mentioned values are determined.

3.3.2.4 Adsorption measurement

Adsorption measurement is performed with an increase stepwise of pressure at constant temperature. As mentioned in the previous section, the recorded balance reading (m_{BAL}) in the measurement needs to be corrected due to the buoyancy effect acting on the sample and the sample container. Thus, the equation of the balance reading is given as below (Rubotherm GmbH, 2005):

$$\Delta m = m^{sc} + m^{s} + m^{A} - \left(V^{sc} + V^{s} + V^{A}\right) \cdot \rho_{H_2} \tag{3.14}$$

where m^{A} and V^{A} is the mass adsorbed and volume of adsorbate, respectively. Rearrange the equation gives:

$$m^{A} = \Delta m - m^{sc} - m^{s} + m^{A} + \left(V^{sc} + V^{s} + V^{A}\right) \cdot \rho_{H_2} \tag{3.15}$$

Hence m^{A} can be determined since all other variables can be calculated. The density of hydrogen, ρ_{H_2} is determined using National Institute of Standards and Technology (NIST) Thermophysical Properties of Hydrogen program.

3.8 Electron Microscope

Electron microscopes (EM) are scientific instruments that use a beam of highly energetic electrons to image the specimens instead of light (Central Facility for Electron Microscopy (CFEM), 2003). This is because light microscopes are limited by the physics of light to 500x or 1000x magnification and a resolution of 0.2 micrometers. The electrons are used since the wavelengths are much shorter than that of lights, which result in higher resolution of images (Davis, 2003). The first construction of the electron microscopy began in 1924 by L. de Broglie who discovered the wave-character of electron rays. Later, the prototype was built by M. Knoll and E. Ruska from Technische Universität Berlin in 1932

(Sengbusch, 2003). By using EMs, the examination of image can yield to the following information (Central Facility for Electron Microscopy (CFEM), 2003):

a. Topography – provides the surface feature and texture of the specimen.
b. Morphology – provides the shape and size of the particles.
c. Composition – provides the elements and compounds of the object
d. Crystallographic information – provides how the atoms are arranged in the object and the arrangements are related to the material properties.

The next section focuses on two examples of EMs that are scanning electron microscopy and transmission electron microscopy.

3.8.1 Scanning electron microscope

Scanning electron microscopy (SEM) uses electron reflected from the surface of specimen to create a three-dimensional image (Davis, 2003). The beam current in the SEM is between 10^{-1} and 10^{-7}Å with beam energy of 200eV-50keV (Wells, 2001). When electron beam strikes on the sample, several photon and electron signals are emitted (Klesel, 2006) as in Figure 3.9. Each signal provides certain information on the specimen. The features of SEM can be seen in Appendix B-1.

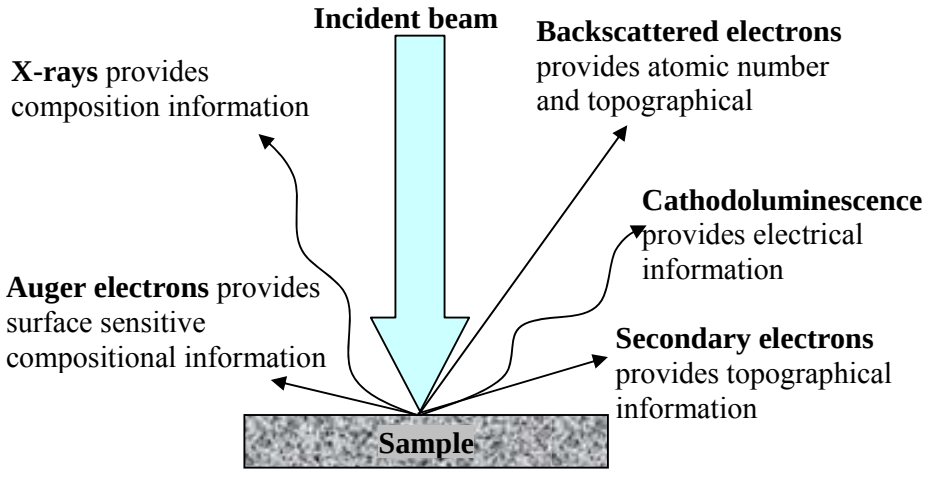

Figure 3.9 Signals from specimen in SEM (Klesel, 2006)

3.8.2 Transmission electron microscope

Transmission electron microscopy (TEM) works the same way as a slide projector except that it shines a beam of electrons (instead of light) through the specimen. Any part that has been transmitted is projected onto a phosphor screen for the user to see (Central Facility for Electron Microscopy (CFEM), 2003). TEM uses high-energy (approximately 100 to 400 keV) electrons to form images of the internal structure of materials. The instrument can provide an image of the internal defect structure from magnifications of 10X to more than 10^6X (Williams, 2001).

Further details of TEM can be found in Appendix B-2. An additional useful feature provided by TEM is that it can display diffraction pattern of the electron beam due to selected area of the material being examined (Blackman, 2005). From the pattern, it gives information on the crystalline structure of the material. Such pattern could identify and differentiate among CNTs and GNFs. Figure 3.10 shows schematic of diffraction patterns on CNT and GNF crystal structure. TEM has been extended in several versions such as high-resolution TEM (HRTEM), high-voltage TEM (HVTEM), and scanning TEM (STEM) to incorporate different types of specimens and imaging options (Williams, 2001).

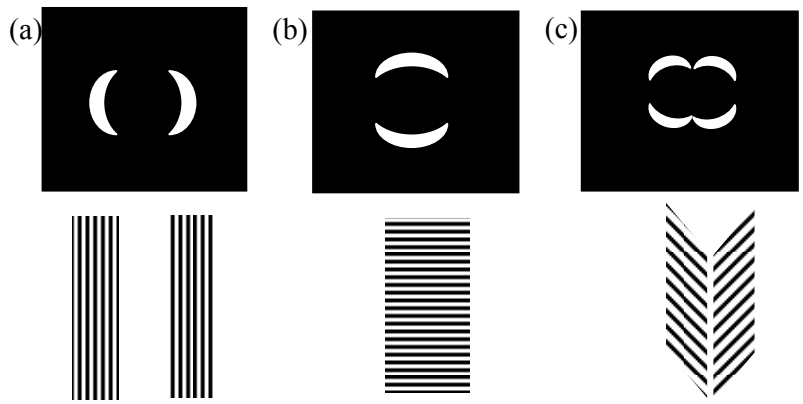

Figure 3.10 Schematic of selected area electron diffraction (SAED) patterns of (a)multiwall nanotubes, (b)platelet; and (c)herringbone crystal structures

3.9 Raman spectroscopy

Raman spectroscopy is named after an Indian physicist, Sir Chandrasekhra Venkata Raman who discovered the Raman effect in 1928 (Singh, 2002). This powerful light scattering technique is used to diagnose the internal structure of molecules and crystals. It is applied in structure determination, multicomponent qualitative analysis, and quantitative analysis (Tissue, 1996).

In general, when a photon imposes on a molecule, three possible things can happen as in Figure 3.11. Due to interaction with the radiation possessing energy E_0, the molecule is lifted up from a ground state to an excited state of higher energy (Tarnowski et al., 2001). The first possibility is that the light can be elastically scattered with no loss in energy since the incident and scattered radiation possess the same frequency. Hence, the change of energy, ΔE is zero (refer to Equation 3.16) and it is known as Rayleigh scattering (Smith et al., 2005):

$$\Delta E = E_0 - E = h \cdot v_0 - h \cdot v_0 = 0 \tag{3.16}$$

where h is the Planck constant and v_0 is the frequency that is the number of waves in the distance light travels in one second.

The second possibility is known as Raman Stokes scattering where some of the energy can be used by the molecule to vibrate and giving off the residual energy in the form of a lower energy photon. Therefore the change of energy is in Equation 3.17 (Smith et al., 2005):

$$\Delta E = E_0 - E = h \cdot v_0 - h \cdot \left(v_0 - v_V\right) = hv_V \tag{3.17}$$

The last possibility is when the molecule losses the energy. The vibrational energy of the molecule is added to the energy of the incident photon, scattering a high-energy photon which is known as Raman anti-Stokes scattering and the change of energy is as follows (Smith et al., 2005):

$$\Delta E = E_0 - E = h \cdot v_0 - h \cdot \left(v_0 + v_V\right) = -hv_V \tag{3.18}$$

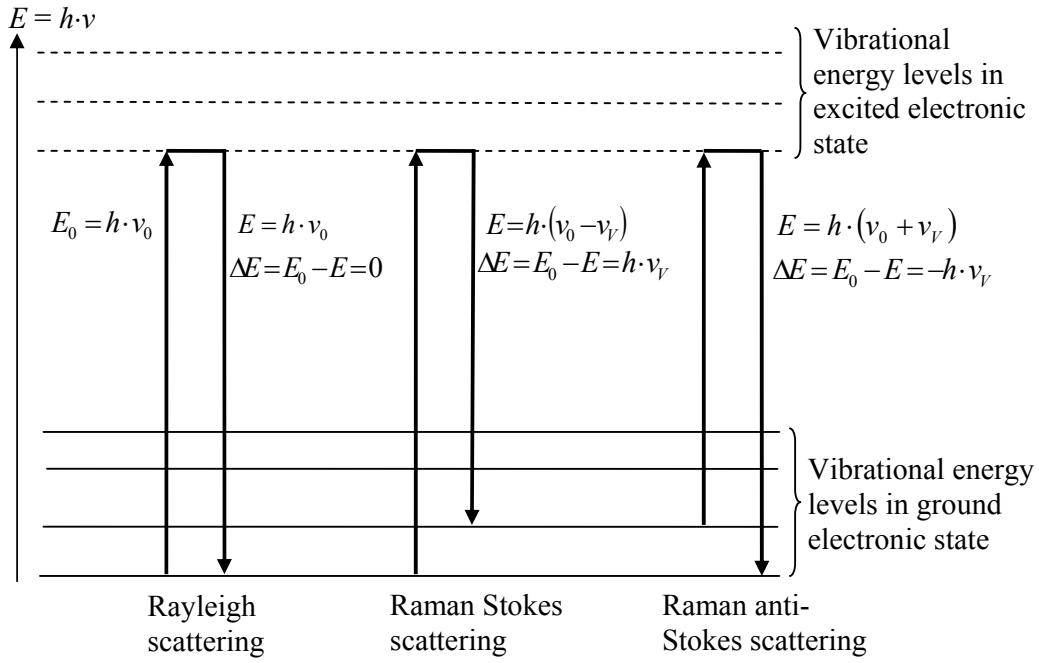

Figure 3.11 Process of resonance Raman scattering (Smith et al., 2005)

The difference in energy between the inelastically scattered photon and the original photon corresponds to the vibrational-mode energy is known as the "Raman shift" that is expressed in cm^{-1} unit. Raman scattered light is frequency-shifted with respect to the excitation frequency, but the magnitude of the shift is independent of the excitation frequency. Thus the Raman shift is an intrinsic property of the sample (Walker, 2002). Raman Stokes scattering is often used in the studies because it has a higher probability for occurrence than Raman anti-Stokes. Unlike infra red (IR) spectroscopy, Raman spectroscopy requires a change in the polarizability of an excited vibrational state of a molecule only (Raman active) (Tarnowski et al., 2001). Therefore, Raman spectroscopy is a complement to IR spectroscopy, which requires a change in dipole moment (non-Raman active excitations). The experimental set up of Raman spectroscopy can be found in Appendix B-3.

Raman spectroscopy has been proven to be a powerful tool to characterize carbon nanomaterials such as carbon nanotubes (CNTs) and graphitic nanofibers (GNF). This is because the resonance phenomena and sensitivity of the tube

structure provides a strong excitation wavelength dependence of the spectra resulting from the electronic band structure (Horiba, 2005). A high laser beam of Raman spectroscopy is so powerful that it is actually burn all impurities such as amorphous carbon and leaves a clean sample. Radial Breathing Mode (RBM) is the most important feature in Raman spectrum for CNT. It is located between 75- 300 cm^{-1} (Horiba, 2005). However, for a specific SWNT, RBM features are between 120 cm^{-1} and 250 cm^{-1} (Jorio et al., 2003). The frequency of the RBM is directly linked to the reciprocal of the nanotube diameter, d_t. For the case of SWNT, the relation is as below:

$$r = 224/d_t \tag{3.19}$$

However, RBM is not suitable for larger diameter tubes. For example in MWNTs, the RBM is too weak to be observed. Another feature is the *D* mode or disorder band which is located between 1330 cm^{-1} and 1360 cm^{-1}. This excitation is expected to be observed in MWNTs. When it is observed in SWNTs, it is assumed that the feature observed is due to defects in the tubes. The next feature known as *G* mode or Tangential Mode (TM). It corresponds to the stretching mode in the graphite plane. This mode is located around 1580 cm^{-1}. The shoulder at higher frequency (1618 cm^{-1}) or *D*' band is typical of defective graphitelike materials and can be smaller in better quality MWNT samples (Jorio et al., 2003).

3.10 X-ray diffractometer

X-ray diffractometer (XRD) is used to reveal detailed information about the chemical composition and crystallographic structure of natural and manufactured materials (Panalytical, 2009). It can determine the crystal structure of an unknown material as well as measure the size, shape and internal stress of small crystalline regions (Moeck, 2004). Details of XRD set up are in Appendix B-4. The distance is known as *d*-spacing. This value can be obtained from Braggs Law which is expressed as (Bruker AXS, 2001):

$$n\lambda = 2d\sin\theta \tag{3.20}$$

where n is the order of reflection and λ is the wavelength of the x-ray. d-spacing of lattice planes depends on the size of its elementary unit cell. It determines the position of a peak. In any XRD peak, the intensity depends on the crystallographic structure, the position of the atoms within the cell and their thermal vibration (Bruker AXS, 2001). Since there are many atomic planes, a coordinate system for the crystal whose unit vector a, b and c are the edges of the unit cell is introduced. The interaxial angles between them are known as α, β and γ. One example of a cubic system can be seen in Figure 3.12, which forms an orthogonal system.

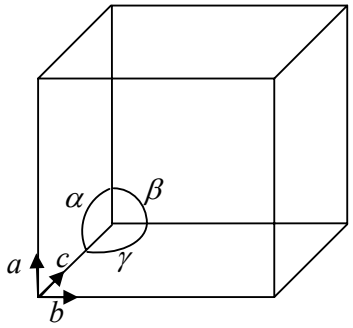

Figure 3.12 A unit cell of a cubic lattice (Bruker AXS, 2001)

The unit cell can be stacked to fill three-dimensional space and there are seven unit-cell shapes that are known as crystal systems as in Table 3.2 (Moeck, 2004).

Table 3.2 Seven crystal systems (Moeck, 2004)

Crystal system	Axis system
Cubic	$a = b = c,\ \alpha = \beta = \gamma = 90°$
Tetragonal	$a = b \neq c,\ \alpha = \beta = \gamma = 90°$
Hexagonal	$a = b \neq c,\ \alpha = \beta = 90°,\ \gamma = 120°$
Rhombohedral	$a = b = c,\ \alpha = \beta = \gamma \neq 90°$
Orthorombic	$a \neq b \neq c,\ \alpha = \beta = \gamma = 90°$
Monoclinic	$a \neq b \neq c,\ \alpha = \gamma = 90°,\ \beta \neq 90°$
Triclinic	$a \neq b \neq c,\ \alpha \neq \beta \neq \gamma \neq 90°$

An atomic plane can be uniquely distinguished by its Miller indices. These Miller indices are the reciprocals of the fractional intercepts which the plane makes

with crystallographics axes (*a*-, *b*- and *c*-axes) and are reduced to the smallest integers with similar ratio (Moeck, 2004; Toney, 1992). Therefore, an (*hkl*) plane intercepts the crystallographic axes at *a*/*h*. *b*/*k* and *c*/*l*. For a crystal in a cubic system, the relationship between the *d*-spacing and the (*hkl*) is as (Toney, 1992) as follows:

$$d = \frac{a_0}{\sqrt{h^2 + k^2 + l^2}} \tag{3.21}$$

where a_0 is the lattice constant of the crystal.

When crystalline is smaller, the parallel planes in it are too small for a sharp diffraction maximum to build up. As a result, the peaks in the diffraction pattern become broadened (Suryanarayana et al., 1998). Apart from crystallite size, the broadening of x-ray diffraction could be due to instrumental effects and lattice strain. Hence, an expression to determine crystallite size, L is defined as (Suryanarayana et al., 1998):

$$L = \frac{k\lambda}{B_{\text{crystallite}} \cos\theta} \tag{3.22}$$

This is a Scherrer formula where $B_{\text{crystalite}}$ is full-width of half-maximum (FWHM) of the peak intensity after correcting of a peak broadening which is caused by diffractometer, λ is the x-ray wavelength, θ is the Bragg angle and k is the shape coefficient for reciprocal lattice point, which is varied from 0.89 and 1.39, depending on (*hkl*) and crystallite size. The Scherrer formula is applicable to a crystallite size less than 1000 Å (Tennyson, 18 May 2007).

3.11 Summary

The study of design of experiment theory following Taguchi approach and the ANOVA used in the analyzing the results are essential in determining the optimum conditions of the experiments. Apart from that, the understanding of basic theory and principles of each analytical instrument and hydrogen measurement equipment are crucial before further analysis can be done.